Science of the Total Environment 721 (2020) 137753

Contents lists available at ScienceDirect

Science of the Total Environment

journal homepage: www.elsevier.com/locate/scitotenv

# Factors affecting co-valorization of fayalitic and ferronickel slags for the production of alkali activated materials

Konstantinos Komnitsas [a,*], Lourdes Yurramendi [b], Georgios Bartzas [c], Vasiliki Karmali [a], Evangelos Petrakis [a]

[a] Technical University of Crete, School of Mineral Resources Engineering, University Campus, Kounoupidiana, 73100 Chania, Greece
[b] Tecnalia, Energy and Environment Division, Mikeletegi Pasealekua 2, E-20009 San Sebastián, Spain
[c] National Technical University of Athens, School of Mining and Metallurgical Engineering, 9 Heroon Polytechniou str., 157 80 Zografos, Athens, Greece

## HIGHLIGHTS

- Alkali-activated materials (AAMs) were produced using three metallurgical slags.
- Use of fayalitic slag (FS), after plasma treatment (FSP) and ferronickel slag (LS)
- Mechanical properties of AMMs were improved when FS and FSP were mixed with LS.
- AMMs from slag mixtures maintained very good structural integrity after firing.
- Alkali activation is a viable option for the co-valorization of different slags.

## GRAPHICAL ABSTRACT

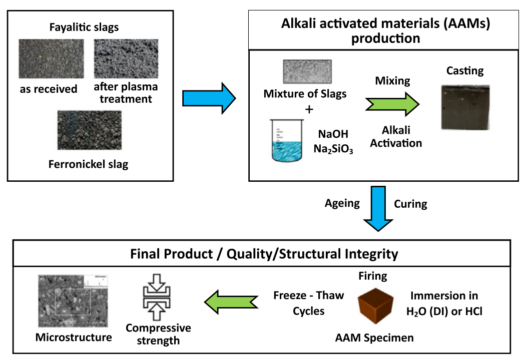


## ARTICLE INFO

*Article history:*
Received 16 January 2020
Received in revised form 12 February 2020
Accepted 4 March 2020
Available online 05 March 2020

Editor: Daniel CW Tsang

*Keywords:*
Metallurgical slags
Alkali activation
Properties
Reactivity of slags
Alkali activated materials (AMMs)

## ABSTRACT

The first objective of this experimental study is the assessment of the alkali activation potential of two types of fayalitic slags, an as-received one (FS) and the one obtained after plasma treatment (FSP) of the initial FS, for the production of alkali activated materials (AAMs). Furthermore, the second objective is the elucidation of the co-valorization potential of FS and FSP slags when mixed with ferronickel (FeNi) slag (LS). The alkaline activating solution used was a mixture of sodium hydroxide (NaOH) and sodium silicate ($Na_2SiO_3$). The effect of various operating parameters, such as $H_2O/Na_2O$ and $SiO_2/Na_2O$ ratios present in the activating solution, curing temperature, curing period and ageing period on the compressive strength, density, water adsorption, porosity and toxicity of the produced AAMs was explored. The structural integrity of selected AAMs was investigated after firing specimens for 6 h at temperature up to 500 °C, immersion in distilled water and acidic solution or subjection to freeze-thaw cycles for a period of 7 or 30 days. The results of this study show that FS- and FSP-based AAMs acquire compressive strength of 44.8 MPa and 27.2 MPa, respectively. When FS and FSP were mixed with LS at 50:50%wt ratios the compressive strength of the produced specimens increased to 64.3 MPa and 45.8 MPa, respectively. Furthermore, selected AAMs produced after co-valorisation of slags retained sufficient compressive strength after firing at 500 °C, 45–68 MPa, and exhibited very low toxicity. These findings prove the alkali activation potential of fayalitic slags as well as their co-valorization with ferronickel slag for the production of AAMs, an approach which is in line with the principles of zero-waste and circular economy.



* Corresponding author.
*E-mail address:* komni@mred.tuc.gr (K. Komnitsas).

https://doi.org/10.1016/j.scitotenv.2020.137753
0048-9697/

## 1. Introduction

The metallurgical industry produces worldwide large quantities of various types of slags that are mainly used in construction applications. Some slags may contain hazardous compounds and their direct use, or uncontrolled disposal, may cause environmental impacts (Agnello et al., 2018; Gee et al., 1997; Muñoz et al., 2018). On the other hand, it has to be underlined that several slags possess beneficial physical and chemical properties and thus their valorization, following the principles of zero waste and circular economy, results in environmental benefits and improves the sustainability of the metallurgical and construction sectors (Bartzas and Komnitsas, 2015; Liu et al., 2019; Mastali et al., 2020; Pasetto et al., 2017; Ouellet-Plamondon and Habert, 2014). Regarding the Portland cement industry, it is mentioned that the adoption of low-carbon binders, namely alkali-activated, carbonate, and belite-ye'elimite-based binders, will play a key role in reducing its carbon footprint (Shi et al., 2019).

Alkali activation is considered a feasible approach and has received great interest over the last 30 years for the valorization of various industrial wastes and the production of materials with amorphous or partially crystalline structure, beneficial physico-chemical properties and higher added value (Davidovits, 1991; Komnitsas et al., 2019a; Kriven et al., 2003; Krivenko and Kovalchuk, 2007; Xu and Van Deventer, 2000). However, it has to be mentioned that alkali activated cement based binders may exhibit some shortcomings that need to be clearly addressed before they effectively compete against Portland cement; these shortcomings mainly include production cost, $CO_2$ emissions and reduced durability due to efflorescence formation, alkali silica reaction and corrosion of reinforced steel (Pacheco-Torgal et al., 2017).

The use of alkali activated materials (AAMs), termed as inorganic polymers or geopolymers, contributes to considerable savings of virgin raw materials and a noticeable reduction of the environmental footprint of various industrial sectors (Duxson et al., 2007; Habert et al., 2011; Komnitsas and Zaharaki, 2007; Komnitsas, 2011; Komnitsas et al., 2019b; Palomo et al., 2014; Passuello et al., 2017). Recent studies on AAMs and various binders also explore their beneficial use in water and wastewater treatment (Alshaaer et al., 2015; Bumanis et al., 2019; Luukkonen et al., 2019), as well as in solidification/stabilization of contaminated sediments and municipal solid waste incinerator fly ash (Chen et al., 2019; Komnitsas, 2016; Wang et al., 2019). Successful alkali activation requires the use of aluminosilicate raw materials, strong alkaline solutions such as NaOH and KOH and a silicate solution such as $Na_2SiO_3$ that is usually added to balance the Si/Al ratio in the reactive paste, which after curing for a few hours at rather mild temperatures (30–90 °C) enables the formation of a matrix with beneficial properties (Bernal et al., 2010; Duxson and Provis, 2008; Khale and Chaudhary, 2007; Peys et al., 2019a; Yip et al., 2005).

During the last years, alkali activation of various types of slags has been widely studied and the results of efforts on upcycling these slags to produce sustainable cementitious binders have been reported in literature. The produced AAMs have various properties depending on the mineralogy and chemistry of the raw slags, the particle size, the synthesis conditions, the silicate modulus in the activating solution and the type of additives used to improve the properties of the produced matrix (Huang et al., 2017; Kaze et al., 2018; Petrakis et al., 2019; Traven et al., 2019; Tchadjie and Ekolu, 2018; Yan et al., 2017). In other studies, mixtures of slags with other waste types including fly ash from power stations, bauxite residues, construction and demolition wastes as well as aluminosilicate minerals such as kaolin or metakaolin in order to regulate the mineralogy of the raw materials have been successfully alkali activated (Furlani et al., 2018; Marjanović et al., 2015; Onisei et al., 2012; Pontikes et al., 2013; Provis and Bernal, 2014).

The ultimate objective of this study is the co-valorization of metallurgical slags with different mineralogy and the optimization of alkali activation conditions for the production of AAMs with beneficial properties.

## 2. Materials and methods

### *2.1. Materials*

The raw materials used in this study were two types of slags, namely a fayalitic slag (FS) produced after pyrometallurgical treatment of copper concentrates in flash smelting furnace in Finland for the production of copper cathodes, copper sulphate and various metal concentrates (Saari et al., 2019) and a slag produced after plasma treatment (FSP) of the previous FS. The plasma treatment was carried out at Tecnalia, Spain, in a pilot plant furnace at 1650 °C with the use of coke as reducing agent and calcium hydroxide as flux. It is mentioned that apart from slag, two more materials were produced, a Zn-rich fly ash and an Fe-rich metallic fraction, which are both marketable products according to their composition (Fig. 1). In addition, in order to investigate the co-valorization potential of different slags for the production of AAMs, a third slag (LS) produced at Larco S.A, in Greece, after pyrometallurgical treatment of nickel laterites in electric-arc furnace for the production of ferronickel (FeNi) was used (Komnitsas et al., 2007).

Prior to use, all slags were pulverized using a Bico type pulverizer (Type UA, Fritsch, Dresden, Germany) and the particle size distribution was obtained with the use of a laser particle size analyzer (Mastersizer S, Malvern Instruments, Malvern, UK). The chemical analysis of the slags was carried out using a Bruker-AXS S2 Range Spectroscopic Fluorescence Spectrometer A (XRF-EDS, Bruker, Karlsruhe, Germany). The particle size distribution and chemical composition in the form of oxides of the three slags are presented in Tables 1 and 2, respectively.

It is observed from Table 1 that the 90% passing size ($d_{90}$) of all slags is less than 50 μm, which is considered adequately fine for efficient alkali activation and the production of AAMs, as indicated in previous studies (Komnitsas et al., 2015).

All slags contain sufficient amounts of $SiO_2$ and $Al_2O_3$ for alkali activation, while their $F_2O_3$ content is also high (Van De Sande et al., 2020). It is also observed that the CaO content in FSP and LS slags is higher compared to FS slag (Table 2).

### *2.2. Synthesis of AAMs*

The alkali activating solution used for the synthesis of AAMs was a mixture of sodium hydroxide (NaOH, Sigma Aldrich) and sodium silicate (7.5–8.5 wt% NaOH and 25.5–28.5 wt% $SiO_2$, Merck). The sodium hydroxide solution was produced by dissolving anhydrous pellets of

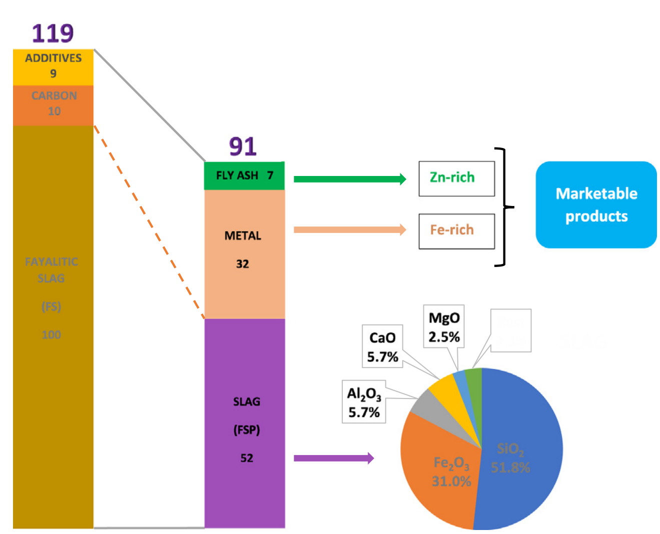


**Fig. 1.** Plasma treatment of FS slag for the production of FSP slag (and two other marketable products), carried out at Tecnalia, Spain (the main chemical composition of FSP slag is also indicated).

**Table 1**
Particle size distribution of the three slags.

| Particle size (μm) | FS | FSP | LS |
|---|---|---|---|
| $d_{90}$ | 48.6 | 41.3 | 45.7 |
| $d_{50}$ | 9.0 | 5.7 | 8.9 |

NaOH in distilled water so that solutions with different molarity (6–10 mol $L^{-1}$, M) were obtained.

The raw materials were mixed with the activating solution under continuous stirring in a laboratory mixer for about 15 min in order to produce a homogeneous paste. Then, the fresh paste was casted in metallic cubic molds (5 cm edge) which were vibrated for a few minutes to remove air. Pre-curing of the reactive paste was carried out at room temperature for 6 h until sufficient hardening was enabled. Then, the produced specimens were sealed in plastic bags to avoid moisture loss and placed in a laboratory oven (Jeio Tech ON-02G, Seoul, Korea) for curing at 40, 60 or 90 °C for 24 h. After curing the specimens were removed from the oven, allowed to cool at room temperature (~20 °C), demoulded and left for ageing for a period of 7 and 28 days. All tests were carried out in triplicate. The AAM codes, the mixing ratios for all materials used as well as the $H_2O/Na_2O$ and $SiO_2/Na_2O$ ratios in the activating solution are presented in Table 3.

The thermal response of selected AAMs was assessed after firing them at 250, 350 and 500 °C in a laboratory furnace (N – 8 L Selecta) for 6 h). Also, the structural integrity of selected AAMs was evaluated by immersing them in various solutions, namely distilled water and acidic solution (1 M HCl) for 7 and 30 days or subjecting them to freeze-thaw cycles using $-18 \pm 5$ °C for 4 h and room temperature ($20 \pm 0.5$ °C) for 12 h as temperature extremes over a period of 7 and 28 days (Standard C1262–10) (ASTM, 2018). Finally, the compressive strength as well as selected physical properties (i.e. porosity, water absorption and apparent density) of selected specimens after each treatment were determined.

### 2.3. Characterization of slags and AAMs

The reactivity of slags was evaluated through leaching tests carried out in 250 mL conical flasks under continuous stirring; 1.0 g of ground solids was added in 100 mL of 8 M NaOH solution and leaching was carried out for 24 h at room temperature (~20 °C). After leaching solid and liquid separation was done using 0.45 μm pore size membrane filters (PTFE, Chromafil). The concentration of Al and Si in solution was determined using an Inductively Coupled Plasma Mass Spectrometry (ICP MS, Agilent 7500 cx) equipped with an Agilent ASX-500 Autosampler.

The chemical analysis of raw materials and the produced AAMs was determined using a Bruker S2 Ranger – energy dispersive X-ray fluorescence spectrometer (ED-XRF, Bruker, Karlsruhe, Germany), while their mineralogical analysis was performed using an X-ray diffractometer with a Cu tube and scanning range from 4° to 70° 2theta (θ), with a step of 0.02°, and 0.2 s/step measuring time (D8-Advance type, Bruker AXS, Karlsruhe, Germany). Data were then qualitatively analyzed with the DiffracPlus Software (EVA *v*. 2006, Bruker, Karlsruhe, Germany) using the PDF database. Fourier transform infrared (FTIR) spectroscopy was carried out for the wavenumber range 400 to 4000 $cm^{-1}$, using a Perkin Elmer Spectrum 1000 spectrometer (Perkin Elmer, Akron, OH, USA), Pellets produced after mixing a pulverized sample of each specimen with KBr at a ratio of 1:100 w/w. The tests were carried out at atmospheric pressure under nitrogen atmosphere, with a flow rate of 100 mL $min^{-1}$ and a heating rate of 10 °C $min^{-1}$. The morphology of the AAMs was assessed by Scanning electron microscopy (SEM) using a JEOL-6380LV scanning microscope (JEOL ltd., Tokyo, Japan) with an Oxford INCA Energy dispersive spectroscopy (EDS) micro analysis system (Oxford Instruments, Abingdon, UK). The compressive strength of the produced AAMs was determined using a MATEST C123N load frame (compression and flexural machine, Matest S.p.A, Treviolo, Bergamo, Italy). The other properties, namely apparent density, porosity and water absorption, of selected AAMs were determined according to the standard BS EN 1936 (BSI, 2007).

**Table 2**
Chemical composition (wt%) of slags.

| Oxide | FS | FSP | LS |
|---|---|---|---|
| $Na_2O$ | 0.5 | 0.6 | – |
| $Fe_2O_3$ | 57.6 | 31.0 | 43.8 |
| $SiO_2$ | 30.1 | 51.8 | 32.7 |
| $Al_2O_3$ | 2.8 | 5.7 | 8.3 |
| $Cr_2O_3$ | 0.06 | 0.40 | 3.1 |
| MgO | 1.3 | 2.5 | 2.8 |
| CaO | 1.0 | 5.7 | 3.7 |
| NiO | 0.2 | – | – |
| $K_2O$ | 0.9 | 1.2 | – |
| $TiO_2$ | 0.2 | 0.3 | – |
| MnO | 0.06 | 0.1 | 0.4 |
| $SO_3$ | 0.4 | 0.5 | 0.2 |
| ZnO | 2.8 | 0.03 | – |
| Total | 97.9 | 99.8 | 95.0 |

**Table 3**
Test details and selected molar oxides in the activating solution.

| AAM Code | NaOH (M) | Slag (wt %) | NaOH (wt %) | $H_2O$ (wt %) | $Na_2SiO_3$ (wt%) | L/S ratio | $H_2O/Na_2O$ | $SiO_2/Na_2O$ |
|---|---|---|---|---|---|---|---|---|
| FS2 | 8 | 81.0 | 2.4 | 7.1 | 9.5 | 0.20 | 17.4 | 1.0 |
| FS3 | 10 | 76.2 | 3.6 | 8.3 | 12.0 | 0.25 | 14.8 | 1.0 |
| FS4 | 6 | 83.7 | 1.3 | 5.2 | 9.8 | 0.18 | 22.5 | 1.5 |
| FS5 | 6 | 85.7 | 1.9 | 7.7 | 4.8 | 0.14 | 20.2 | 0.7 |
| FSP1 | 6 | 82.7 | 2.6 | 10.4 | 4.3 | 0.17 | 19.5 | 0.4 |
| FSP2 | 8 | 81.1 | 3.6 | 10.6 | 4.7 | 0.18 | 14.9 | 0.4 |
| FSP3 | 10 | 80.3 | 4.5 | 10.2 | 4.9 | 0.18 | 11.9 | 0.4 |
| FSP4 | 10 | 82.4 | 2.7 | 6.1 | 8.8 | 0.17 | 14.6 | 0.9 |
| FSP5 | 10 | 81.4 | 3.6 | 8.1 | 7.0 | 0.18 | 13.1 | 0.6 |
| LS | 8 | 83.2 | 2.1 | 6.3 | 8.4 | 0.17 | 17.4 | 1.0 |
| FS10LS90 | 8 | 83.5 | 2.1 | 6.2 | 8.2 | 0.17 | 17.4 | 1.0 |
| FS30LS70 | 8 | 82.6 | 2.2 | 6.5 | 8.7 | 0.18 | 17.4 | 1.0 |
| FS40LS60 | 8 | 81.9 | 2.3 | 6.8 | 9.0 | 0.19 | 17.4 | 1.0 |
| FS50LS50 | 8 | 81.1 | 2.4 | 7.1 | 9.4 | 0.20 | 17.4 | 1.0 |
| FSP10LS90 | 10 | 86.7 | 2.0 | 4.6 | 6.7 | 0.13 | 14.6 | 0.9 |
| FSP30LS70 | 10 | 82.4 | 2.7 | 6.2 | 8.7 | 0.18 | 14.6 | 0.9 |
| FSP40LS60 | 10 | 79.0 | 3.2 | 7.3 | 10.5 | 0.22 | 14.6 | 0.9 |
| FSP50LS50 | 10 | 75.0 | 3.8 | 8.7 | 12.47 | 0.27 | 14.6 | 0.9 |

## 3. Results and discussions

### 3.1. Characterization of slags

The reactivity of slags which indicates their alkali activation potential was assessed after leaching with an 8 mol $L^{-1}$ NaOH solution. Table 4 shows the concentration of Al and Si in the final solution derived after solid: liquid separation, as well as the respective Si/Al ratios. It is seen from this data that LS exhibits the highest reactivity, as indicated by the concentration of Si and Al in the leaching solution, which is 332.5 and 99.1 mg $L^{-1}$, respectively. The high reactivity of ferronickel slag has been also shown in earlier studies (Zaharaki and Komnitsas,

**Table 4**
Concentration of Si, Al and Si/Al ratios in solution after leaching[a].

| Raw material | Si (mg $L^{-1}$) | Al (mg $L^{-1}$) | Si/Al |
|---|---|---|---|
| FS | 139.5 | 14.5 | 9.6 |
| FSP | 100.0 | 23.9 | 4.2 |
| LS | 332.5 | 99.1 | 3.4 |

[a] Leaching with 8 mol $L^{-1}$ NaOH solution for 24 h.

2009). The two fayalitic slags, namely FS and FSP, exhibit lower reactivity since the concentrations of Si and especially Al are much lower, compared to the respective concentrations obtained after leaching of the LS slag; however, their reactivity is considered sufficient for alkali activation. Based on this data, the Si/Al ratios in solution are 9.6, 4.2 and 3.4 for FS, FSP and LS, respectively.

The XRD patterns of all slags are presented in Fig. 2. Magnetite ($Fe_3O_4$) and fayalite ($Fe_2SiO_4$) were the main phases detected in FS, while clinoferrosilite ($FeSiO_3$) was mainly detected in FSP (the detected graphite (Gr) corresponds to traces of residual carbon from the addition made in the pilot for the carbo-reduction plasma reaction). The main mineralogical phases present in LS were magnetite ($Fe_3O_4$), quartz ($SiO_2$), anorthite ($CaAl_2Si_2O_8$), chromite ($FeCr_2O_4$), cristobalite ($SiO_2$), forsterite ($Mg_2SiO_4$), fayalite ($Fe_2SiO_4$) and tridymite ($SiO_2$). It is also mentioned that LS has high amorphous content (~50%) denoted by the broad hump shown between 2θ 25–40$^0$, as also indicated in previous studies (Komnitsas et al., 2009; Zaharaki et al., 2010).

The FTIR spectra of slags FS, LS and FSP are presented in Fig. 3. Regarding FS, the rocking band at 457 cm$^{-1}$ is characteristic of fayalitic slags and corresponds to in plane Si – O bending and Al – O linkages as well as bending Si – O– Si and O – Si – O vibrations (Komnitsas et al., 2013; Komnitsas et al., 2015; Yip et al., 2008). An additional peak associated with the stretching vibrations of T-O-T (T = Si, or Al) bonds is also seen at 575 cm$^{-1}$, while the bands at 689 cm$^{-1}$ and 876 cm$^{-1}$ are attributed to the bending modes of $CO_3^{-2}$ (Komnitsas et al., 2019a, 2019b). The narrow band at 505 cm$^{-1}$, which is typical of the Fe—O stretching vibrations, is due to the presence of magnetite in LS, as also confirmed by XRD analysis (Muthuvel et al., 2019). The major band observed at 961 cm$^{-1}$ represents the Si—O asymmetric stretching vibrations with its wide broadness indicating the high glassy/vitreous content present in FS and LS slags (Chen et al., 2020; Komnitsas et al., 2009). The FTIR spectrum of LS also shows two narrow bands at 2845 cm$^{-1}$ and 2918 cm$^{-1}$, typical of symmetric and asymmetric –$CH_2$- stretching vibrations, respectively (Li et al., 2019), while the two bands at 1525 cm$^{-1}$ and 2370 cm$^{-1}$ in the FSP are attributed to the atmospheric carbonation (Gao et al., 2014; Komnitsas et al., 2015). Finally, the broad bands at 1382 cm$^{-1}$ and 3423 cm$^{-1}$, which are related to the presence of water, are due to bending and stretching vibrations of O—H bonds, respectively (Maragkos et al., 2009).

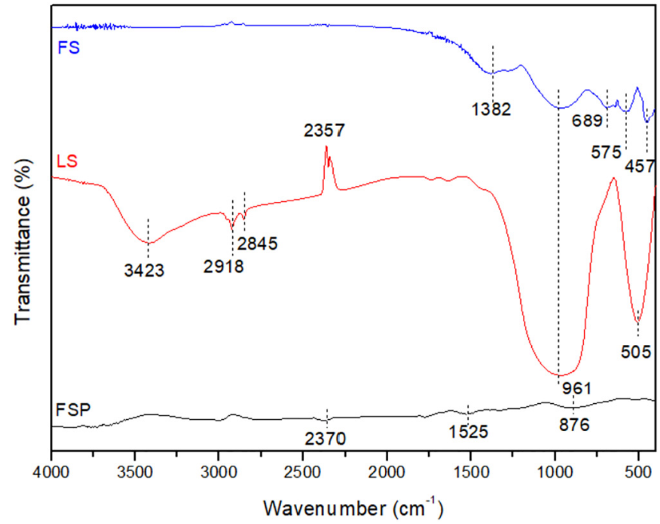


**Fig. 3.** FTIR spectra of FS, FSP and LS slags.

### 3.2. Factors affecting the compressive strength of the produced AAMs

#### 3.2.1. Effect of $H_2O/Na_2O$ molar ratio in the activating solution and ageing period

Fig. 4 presents the compressive strength of the AAMs produced from FS (Fig. 4a) and FSP (Fig. 4b), after curing at 90 °C, as a function of $H_2O/Na_2O$ molar ratio in the activating solution and ageing period (7 or 28 days). The $SiO_2/Na_2O$ molar ratio in the activating solution was kept constant at 1.00 in this series. It is seen that as the $H_2O/Na_2O$ molar ratio decreases from 21.6 to 14.8, the compressive strength of the produced AAMs also decreases, while the increase of ageing period from 7 to 28 days has only a minor beneficial effect. The maximum compressive strength recorded after a curing period of 28 days, was 28.0 MPa, when the $H_2O/Na_2O$ ratio was 21.6. On the other hand, when FSP was used as raw material (Fig. 4b), the decrease in $H_2O/Na_2O$ molar ratio from 19.5 to 11.9, resulted in a noticeable increase in the compressive strength of the produced AAMs. The maximum

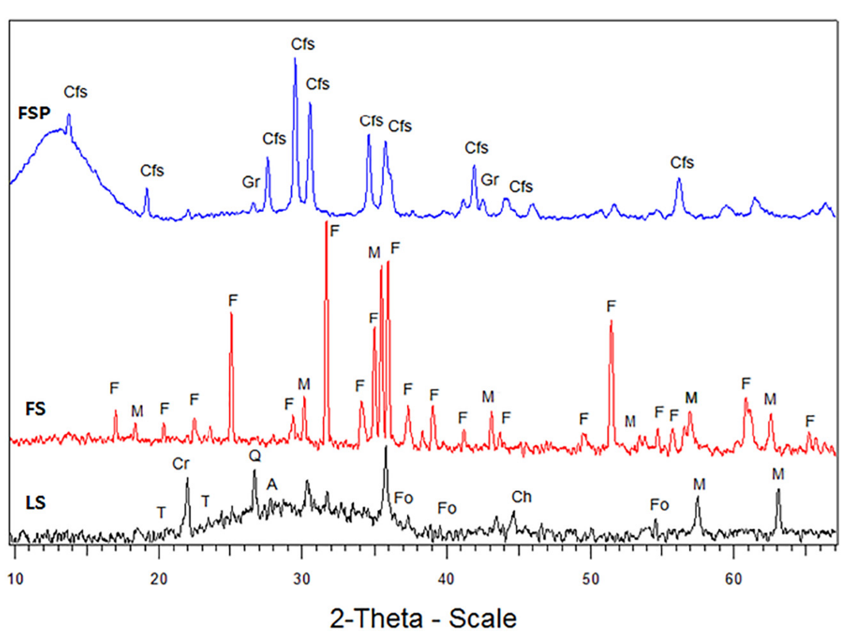


**Fig. 2.** XRD patterns of slags FS, FSP and LS. Phases identified are: anorthite (A), clinoferrosilite (Cfs), chromite (Ch), cristobalite (Cr), fayalite (F), forsterite (Fo), graphite (Gr), magnetite (M), quartz (Q), tridymite (T).

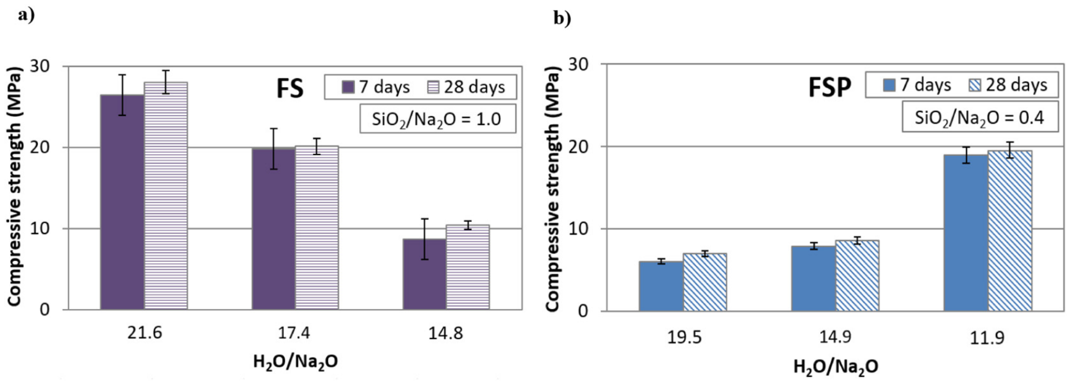


**Fig. 4.** Effect of $H_2O/Na_2O$ molar ratio in the activating solution and ageing period on the compressive strength of (a) FS- and (b) FSP-based AAMs (pre-curing time 6 h, curing temperature 90 °C, curing period 24 h; error bars indicate the standard deviation of measurements obtained from three specimens).

compressive strength recorded was 19.5 MPa when the $H_2O/Na_2O$ ratio was 11.9. It is noted that the $SiO_2/Na_2O$ molar ratio in alkaline solution in this series was kept constant at 0.4. As in the previous case, the effect of the ageing period was negligible.

It is known that the $H_2O/Na_2O$ ratios plays major role during alkali activation; low ratio indicates excess of $OH^-$ ions which may remain unreacted and result in the production of specimens with lower strength, whereas high ratio may indicate either deficiency of $OH^-$ ions or excess of water which may also remain unreacted under specific synthesis conditions. The optimum $H_2O/Na_2O$ ratio in each case depends also on the mineralogy of the precursor and the rate of the reaction between the raw material and the alkaline solution, as indicated in earlier studies (Komnitsas et al., 2019a, 2019b; Soultana et al., 2019; Zaharaki and Komnitsas, 2009).

The results regarding alkali activation of these two slags may be explained by considering their mineralogy as well as the dissolution of Si and Al from the raw materials in alkaline conditions as presented in Table 4. FS exhibits higher activation potential since its Si/Al ratio in the alkaline solution is more than two times higher compared to the respective ratio obtained after leaching of FSP. It is also possible that the reactivity of FSP slag has reduced after plasma treatment.

### 3.2.2. Effect of curing temperature

The compressive strength of the produced AAMs, as a function of curing temperature (40, 60 or 90 °C), when FS or FSP was used as precursor is presented in Fig. 5a and b, respectively. In this series, the $SiO_2/Na_2O$ molar ratio was kept at 1 and 0.4 for FS and FSP respectively, as shown in Fig. 4. It is seen from these results that temperature has a major beneficial effect on the compressive strength of the AAMs produced from both slags, which increases by more than 5 times when the curing temperature increases from 40 to 90 °C. The maximum values of compressive strength obtained after an ageing period of 7 days were 26.5 and 18.9 MPa for FS- and FSP-based AAMs, respectively. It is also mentioned that the weight loss of the specimens during curing increases with increasing temperature from 2 wt% to almost 6 wt % over the temperature range investigated.

It is well known from previous studies, that higher curing temperature accelerates the rate of reactions between the precursors and the activating solution and improves condensation and re-solidification so that more aluminosilicate bonds are formed, a better microstructure is developed and the matrix acquires more beneficial mechanical properties (Soultana et al., 2019; Zaharaki et al., 2016). On the other hand, it should be mentioned that special care should be taken during curing at higher temperature in order to avoid fast evaporation of water which may result in incomplete alkali activating reactions (Gebregziabiher et al., 2016; Sindhunata et al., 2006; Yuan et al., 2016).

### 3.2.3. Effect of $SiO_2/Na_2O$ molar ratio in the activating solution

Fig. 6 shows the compressive strength of the AAMs produced from FS (Fig. 6a) and FSP (Fig. 6b) as a function of $SiO_2/Na_2O$ molar ratio in the alkaline solution, using a curing temperature of 90 °C and an ageing period of 7 days. The respective $H_2O/Na_2O$ ratios are also shown for both series; these ratios are slightly different in each case as indicated in Table 3.

The maximum values of the compressive strength obtained were 44.8 MPa for FS-based AAMs with $SiO_2/Na_2O$ molar ratio of 1.5, while when FSP was used the compressive strength was 27.2 MPa with $SiO_2/Na_2O$ molar ratio of 0.9. It is seen in both cases that the compressive strength of the produced AAMs decreases with decreasing $SiO_2/Na_2O$ molar ratios and this effect is more noticeable for FSP-based specimens. This is mainly due to the fact that when lower $SiO_2/Na_2O$ molar ratios are used less Si ions are available to react and form Si-O-Si

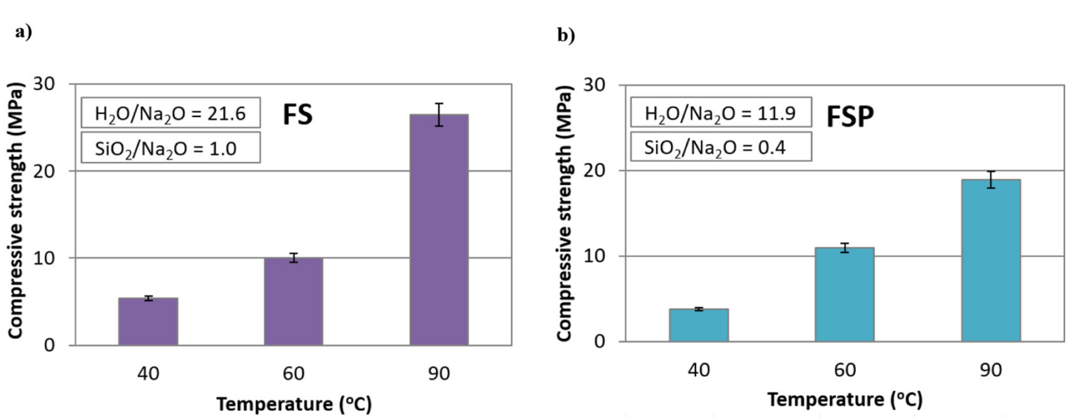


**Fig. 5.** Effect of curing temperature on the compressive strength of (a) FS- and (b) FSP-based AAMs (pre-curing time 6 h, curing period 24 h, ageing period 7 days; error bars indicate the standard deviation of measurements obtained from three specimens).

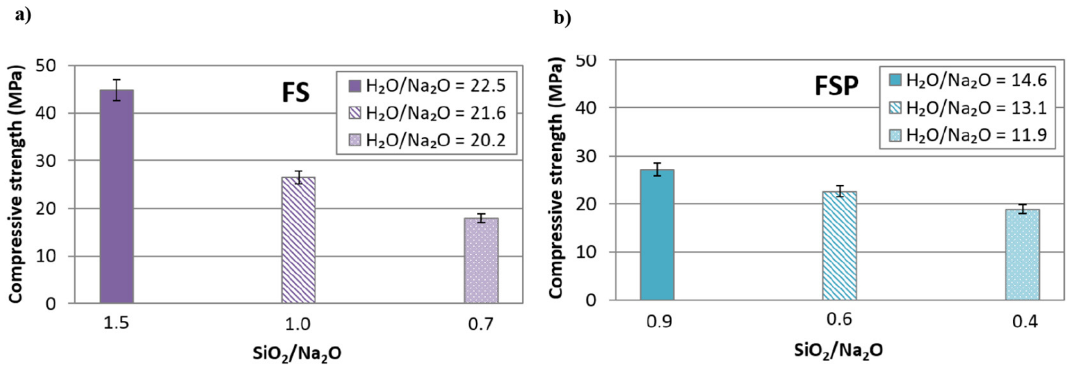


**Fig. 6.** Effect of $SiO_2/Na_2O$ ratio in the activating solution on compressive strength of (a) FS- and (b) FSP-based AAMs (pre-curing time 6 h, curing temperature 90 °C, curing period 24 h, ageing period 7 days; error bars indicate the standard deviation of measurements obtained from three specimens).

bonds and thus specimens with decreased strength are obtained (Gao et al., 2014; Komnitsas et al., 2009). On the other hand, it is known that excess of NaOH in the activating solution may cause early precipitation of aluminosilicate gel or reduced dissolution of Si and Al from the precursor and formation of less oligomers, factors which reduce the compressive strength (Gao et al., 2014; Lee and van Deventer, 2002; Zhang et al., 2009). Also, excess of $Na_2SiO_3$, which is a liquid with high viscosity, may hinder the rate of reactions between the precursors and the activating solution so that the compressive strength is reduced (Yuan et al., 2016).

### 3.2.4. Potential of co-valorization of fayalitic and FeNi slags

In order to assess the potential of slag co-valorization through alkali activation, precursors obtained by mixing FS and FSP with different ratios of LS were used, since as mentioned earlier LS exhibits higher reactivity during alkali activation.

Fig. 7 presents the compressive strength obtained for specimens produced by mixing FS with LS at ratios 10:90, 30:70, 40:60 and 50:50. The synthesis conditions used for the alkali activation of the mixtures were pre-curing period 6 h, curing period 24 h, curing temperature 90 °C and ageing period 7 days. The ratios $H_2O/Na_2O$ and $SiO_2/Na_2O$ in the activating solution were 17.4 and 1.0 respectively. In the same figure the compressive strength of control specimens produced after alkali activation of each slag, namely FS and LS, are also given for comparison.

Experimental results prove the beneficial effect of LS addition in the initial mixture on the subsequent alkali activation, given that the AAMs produced after alkali activation of LS acquire a compressive strength of 80 MPa. It is seen that the specimens produced after alkali activation of all combinations examined acquire very high compressive strength which reaches 64.3 MPa also in the case when the mixing ratio FS:LS is 50:50. This value is almost 70% higher compared to the value recorded for the AAM produced using only FS as precursor. It is also important to mention that almost no loss of strength is noted for the specimens produced from FS:LS mixing ratios 10:90 and 30:70.

Fig. 8 presents the compressive strength obtained from specimens produced by mixing FSP with LS at ratios and synthesis conditions similar as in the previous case. In the same figure the compressive strength of control specimens produced after alkali activation of each slag, namely FSP and LS, are also given for comparison. The ratios $H_2O/Na_2O$ and $SiO_2/Na_2O$ in the activating solution were 14.6 and 0.9, respectively.

Experimental results also in this case prove the beneficial effect of LS addition in the initial mixture on the subsequent alkali activation. It is seen that the specimens produced after alkali activation of all combinations tested acquire very high compressive strength which reaches 45.8 MPa also in the case when the mixing ratio FSP:LS is 50:50. This value is 49% higher compared to the value recorded for the AAM produced from FSP only.

The results of this series prove the high co-valorization potential for both fayalitic and ferronickel slags. Based on this data, AAMs produced using a mixture consisting of 30 wt% FSP and 70 wt% LS, which was alkali activated under the optimum conditions, namely $SiO_2/Na_2O$ 0.9, curing temperature 90 °C, curing period 24 h and ageing period 7 days were selected to study their structural integrity.

### 3.3. Structural integrity and toxicity of AAMs FS30LS70 and FSP30LS70

This section investigates the structural integrity of AAMs FS30LS70 and FSP30LS70 which represent specimens produced using the optimum synthesis conditions in the frame of slags co-valorization. In particular, Fig. 9 shows the evolution of the compressive strength of both

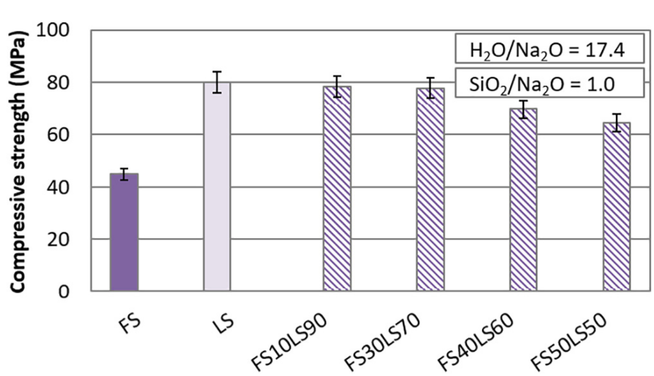


**Fig. 7.** Effect of mixing proportions of FS and LS on the compressive strength of FSLS-based AAMs (pre-curing time 6 h, curing period 24 h, curing temperature 90 °C, ageing period 7 days; error bars indicate the standard deviation of measurements obtained from three specimens).

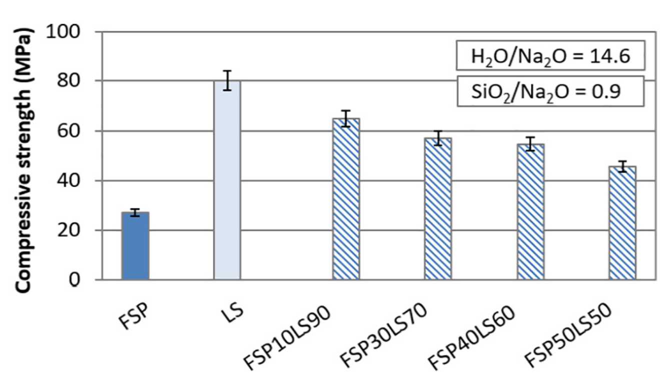


**Fig. 8.** Effect of mixing proportions of FSP and LS on the compressive strength of FSPLS-based AAMs (pre-curing time 6 h, curing period 24 h, curing temperature 90 °C, ageing period 7 days; error bars indicate the standard deviation of measurements obtained from three specimens).

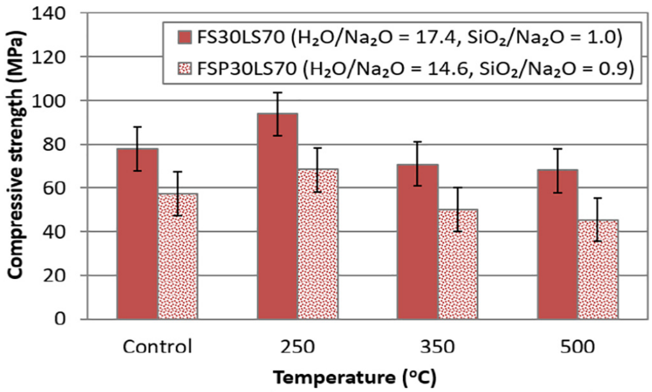


**Fig. 9.** Compressive strength of FS30LS70 and FSP30LS70 AAMs after firing between 250 and 500 °C; synthesis conditions: pre-curing time 6 h, curing period 24 h, curing temperature 90 °C, ageing period 7 days; error bars indicate the standard deviation of measurements obtained from three specimens.

AAMs after firing at 250, 350 and 500 °C for 6 h, while Fig. 10 presents the evolution of compressive strength after their immersion in distilled water and 1 M HCl for a period of 7 and 30 days as well as after the implementation of freeze-thaw cycles, using $-18 \pm 5$ °C and room temperature (~$24 \pm 5$ °C), as temperature extremes over a period of 7 and 28 days. The compressive strength of the control specimens is also shown for comparison.

Fig. 9 shows that the response of both AAMs to firing is good and FS30LS70 exhibits better behavior since its initial strength was higher. More specifically, the compressive strength of FS30LS70 specimen increases by ~20% to 94 MPa after firing at 250 °C, due to volumetric shrinkage (5.0%), and drops slightly by ~12% to 68 MPa after firing at higher temperatures up to 500 °C. Similar behavior is seen for FSP30LS70 which after firing at 500 °C retains a compressive strength of 45 MPa. The compressive strength after firing at higher temperatures, e.g. 800 °C, drops to less than 15 MPa (data not shown), due to phase transformations, deterioration of the structural integrity of the specimens as a result of the decomposition of Si–O–Al and Si–O–Si bonds, and the development of microcracks. It is thus deduced that AAMs produced after firing can be potentially used as medium fire-resistant materials (Abdel-Ghani et al., 2018; Zaharaki and Komnitsas, 2012; Komnitsas et al., 2019a, 2019b).

On the other hand, both specimens exhibit also very good to good behavior after immersion in distilled water or 1 M HCl, respectively for a period of 7 and 30 days. More specifically, immersion in distilled water affects only marginally the compressive strength of the specimens, even after a period of 30 days, whereas immersion in HCl solution for 7 days results in a decrease of compressive strength to 65 MPa for FS30LS70 (Fig. 10a) and 45 MPa for FSP30LS70 (Fig. 10b), respectively. Additional retention of both AAMs in HCl solution for 30 days results in higher drop of compressive strength to 45 MPa and 30 MPa for FS30LS70 and FSP30LS70, respectively. Even though this loss of strength is considered big, it is important to mention that both specimens retain a substantial final strength under such harsh conditions.

Regarding the effect of freeze-thaw cycles for 7 and 30 days, it is seen that both specimens respond very well and that the decrease in strength after 30 cycles is only marginal to 67 MPa for FS30LS70 (14% decrease) and 50 MPa for FSP30LS70 (12% decrease), respectively.

Several studies pertinent to the structural integrity of AAMs using as precursors various types of slags or construction and demolition wastes (i.e. bricks and tiles) have been carried out. Komnitsas et al. (2015) showed that the final compressive strength of brick-based or concrete-based AAMs is slightly affected, while the final compressive strength of tile-based AAMs is severely affected when subjected to freeze–thaw cycles for 1 or 2 months. Mohamed (2019) showed that the alkali-activated slag concrete demonstrates generally better resistance to freeze-thaw compared to Ordinary Portland Concrete (OPC). Luukkonen et al. (2018) studied the freeze-thaw resistance of blast furnace slag mortar specimens and showed that they could withstand 120 cycles.

Finally, Table 5 shows the properties, namely porosity (%), water absorption (%) and density (kg $m^{-3}$) of selected AAMs, i.e. FS, FSP, LS, FS30LS70, FSP30LS70 as well as the last two after firing at 250 °C and 500 °C. All AAMs examined were produced using the optimum synthesis conditions, as shown in the previous graphs. In this table also the compressive strength of these AAMs is also shown.

It is seen from this data that the main differences were observed for porosity and density. It is observed that the porosity was 10.8% for FS4 specimen and decreased to 7.3% for FS30LS70 after firing at 250 °C. A similar trend was observed for water absorption which decreased from 3.8% to 3.2%. On the other hand, by taking into consideration the same AAMs the density increased from 2330 to 4330 kg $m^{-3}$.

Finally, it is mentioned that the solubilisation of heavy metals from FSP, LS and all produced AAMs is well below all available limits, as indicated by the application of TCLP (US EPA, 1992), EN 12457-3 (2002) and NEN 7341 (1995) tests. The only raw material that exhibited some toxicity was the original fayalitic slag (FS) and only in terms of Zn, due to its relatively high content of ZnO (2.80%wt), as shown in Table 2. The application of the TCLP test on FS indicated that Zn concentration in the extract was 10.8 mg $L^{-1}$ but no limit is indicated for this metal by this specific test. The application of the EN 12457-3 test indicated that Zn solubilisation was 63 mg $kg^{-1}$ and based on this value FS as a waste can be only disposed at a landfill that accepts hazardous wastes. The application of NEN test indicates that Zn exhibits noticeable solubilisation,

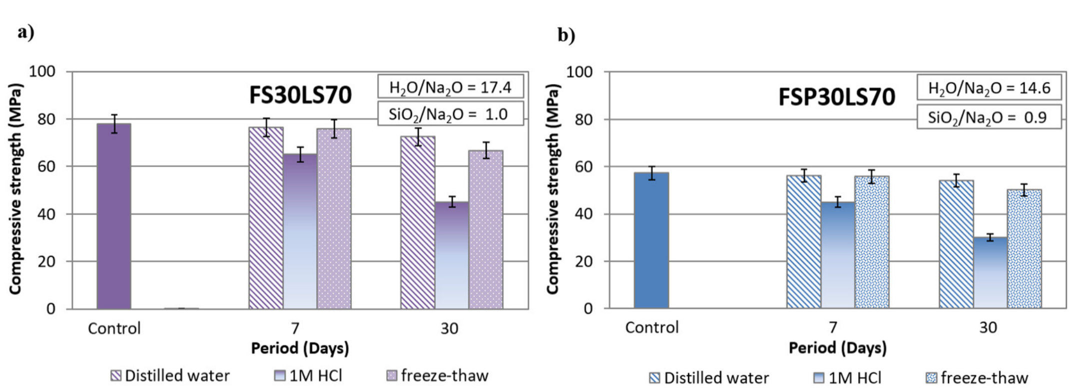


**Fig. 10.** Compressive strength of (a) FS30LS70 and (b) FSP30LS70 AAMs after immersion in distilled water and 1 M (mol $L^{-1}$) HCl and implementation of freeze-thaw cycles for 7 and 30 days; synthesis conditions: pre-curing time 6 h, curing period 24 h, curing temperature 90 °C, ageing period 7 days; error bars indicate the standard deviation of measurements obtained from three specimens.

**Table 5**
Physical properties of selected AAMs.

| AAM code | Compressive strength (MPa) | Water absorption (%) | Porosity (%) | Density ($kg/m^3$) |
|---|---|---|---|---|
| FS | 44.8 | 3.8 | 10.8 | 2330 |
| FSP | 27.2 | 4.0 | 9.4 | 2400 |
| LS | 80.1 | 3.0 | 8.0 | 2580 |
| FS30LS70 (control) | 77.9 | 3.2 | 8.6 | 2640 |
| FS30LS70 after firing at 250 °C | 93.9 | 3.2 | 6.3 | 4330 |
| FS30LS70 after firing at 500 °C | 67.2 | 3.9 | 10.3 | 2650 |
| FSP30LS70 (control) | 57.3 | 2.3 | 8.5 | 3754 |
| FSP30LS70 after firing at 250 °C | 68.3 | 3.8 | 8.8 | 3800 |
| FSP30LS70 after firing at 500 °C | 45.4 | 3.8 | 9.2 | 3428 |

since its concentration in the leachate is 355 mg $kg^{-1}$ at pH 4 and 238,355 mg $kg^{-1}$ at pH 7; however, it has to be taken into account that this test is carried out using high L/S ratio, 50:1, and that no limit is again indicated for this metal. So, alkali activation of these wastes apart of their co-valorisation and the synthesis of new products that can be used as binders or construction materials, also results in reduction of their toxicity, in case that such toxicity exists.

### 3.4. Mineralogy – microstructure of selected AAMs

#### 3.4.1. XRD analysis

Fig. 11 presents the XRD patterns of selected AAMs, namely FS30LS70 before and after firing at 250 °C for 6 h, as well as the patterns of raw FS and LS for comparison. It is observed that the main mineral phases, namely magnetite ($Fe_3O_4$) and fayalite ($Fe_2SiO_4$) present in FS30LS70 are also present after its firing. It is also observed that silicon containing phases, such as quartz, cristobalite and tridymite present in the raw materials are not detected in the produced AAMs, due to their dissolution after the attack of the raw materials by the activating solution. Finally, it is seen that the intensities of the crystalline phases of fayalite and magnetite present in the produced AAMs are in general lower than the ones present in the raw slags. The lower intensities of these dominant phases identified in the AMMs indicate that they partially participate in the reactions and thus confirm to some extent the degree of polymerization (Peys et al., 2019b).

#### 3.4.2. FTIR analysis

Fig. 12 presents the FTIR spectra of selected AAMs, namely FS30LS70 before and after firing at 250 °C for 6 h, as well as the FS and LS for comparison. The FTIR spectra of the AAMs indicated that polymerization took place and has resulted in the increase of the compressive strength. In this context and in line with XRD results (Fig. 11), the disappearance of major bands in the 450–650 $cm^{-1}$ range, which are attributable to characteristic T–O–T (T = Si, or Al) deformation vibrations, suggests that the activating solutions were effective in attacking the glassy content of the raw slags and thus, most part of the dissolved aluminosilicate content has participated in the synthesis of the AAMs (Bernal et al., 2011). Moreover, the FTIR spectra of the AMMs show a slight shift to higher wavenumbers for most vibration bands compared to raw slags, which is typically attributed to the higher Si content in the C–S–H gel and the higher degree of polymerization (Ravikumar and Neithalath, 2012). In particular, a shift of the rocking band at 457 $cm^{-1}$ in the FS towards higher wavenumber (465 $cm^{-1}$) along with a significant reduction in its intensity in the examined AAMs is observed. Another explanation that is proposed, apart from the higher Si content of the inorganic matrix, is that the Fe present in the raw slag partly oxidizes to $Fe^{3+}$ after alkali activation and subsequently decreases the amount of non-bridging oxygens available for the silicate network (Peys et al., 2019a, 2019b; Van De Sande et al., 2020). In this case, higher degree of silicate polymerization is achieved and the Si—O stretching band at 961 $cm^{-1}$ present in the spectra of the raw slags shifts to higher wavenumbers in FS30LS70, i.e. 1017 $cm^{-1}$ and 1021 $cm^{-1}$ before and after firing at 250 °C for 6 h, respectively. Finally, the weaker bands present at 1630 $cm^{-1}$ and 3423 $cm^{-1}$ in the raw LS and attributed to the characteristic H–OH– bending and stretching vibrations of O—H are shifted to broader and more intense bands located at 1633 $cm^{-1}$ and 3450 $cm^{-1}$ in both AAMs, respectively.

#### 3.4.3. SEM analysis

Back-scattered electron (BSE) images of selected AAMs, namely FS30LS70 before and after firing at 250 °C for 6 h are shown in Fig. 13 (a-d). As shown in XRD patterns, SEM analysis of the polished AAM surfaces along with EDS point analyses revealed that fayalite and magnetite particles were the major mineralogical phases identified after alkali activation. Other phases such as chromite occurred as drop-like inclusions, while silicates such as forsterite and quartz were also detected in some places (Fig. 13 b and d). Regarding the microstructure of both AAMs, no

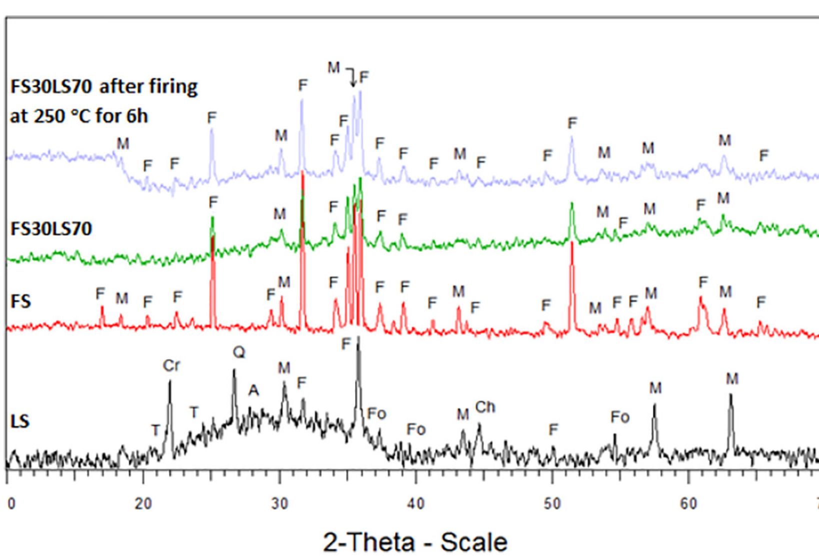


**Fig. 11.** XRD patterns of raw LS and FS slags, as well as AAMs FS30LS70 before and after firing at 250 °C for 6 h - phases identified are: anorthite (A), chromite (Ch), cristobalite (Cr), fayalite (F), forsterite (Fo), magnetite (M), quartz (Q), tridymite (T).

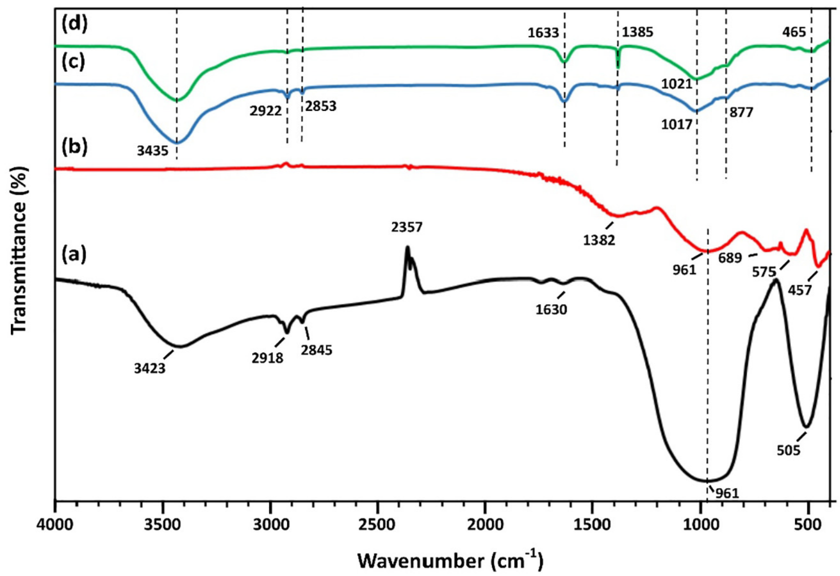


**Fig. 12.** FTIR spectra of raw slags, namely (a) LS and (b) FS, as well as AAMs (c) FS30LS70 before and (d) FS30LS70 after firing at 250 °C for 6 h.

signs of cracks were observed along the cross sectional interfaces examined as a result of the strong bonds that formed after the reactions between the slag particles (mostly fayalite) and the alkaline activators ($Na_2SiO_3$ and NaOH). In this context, the presence of inorganic polymeric gels (G1 and G2) containing Ca, Al, Si, Fe, Mg and Na and surrounded by radically dissolved particles of fayalite and quartz after alkali-activation were identified in FS30LS70 before (Fig. 13b) and after firing (Fig. 13d), respectively. However, the FS30LS70 AAM

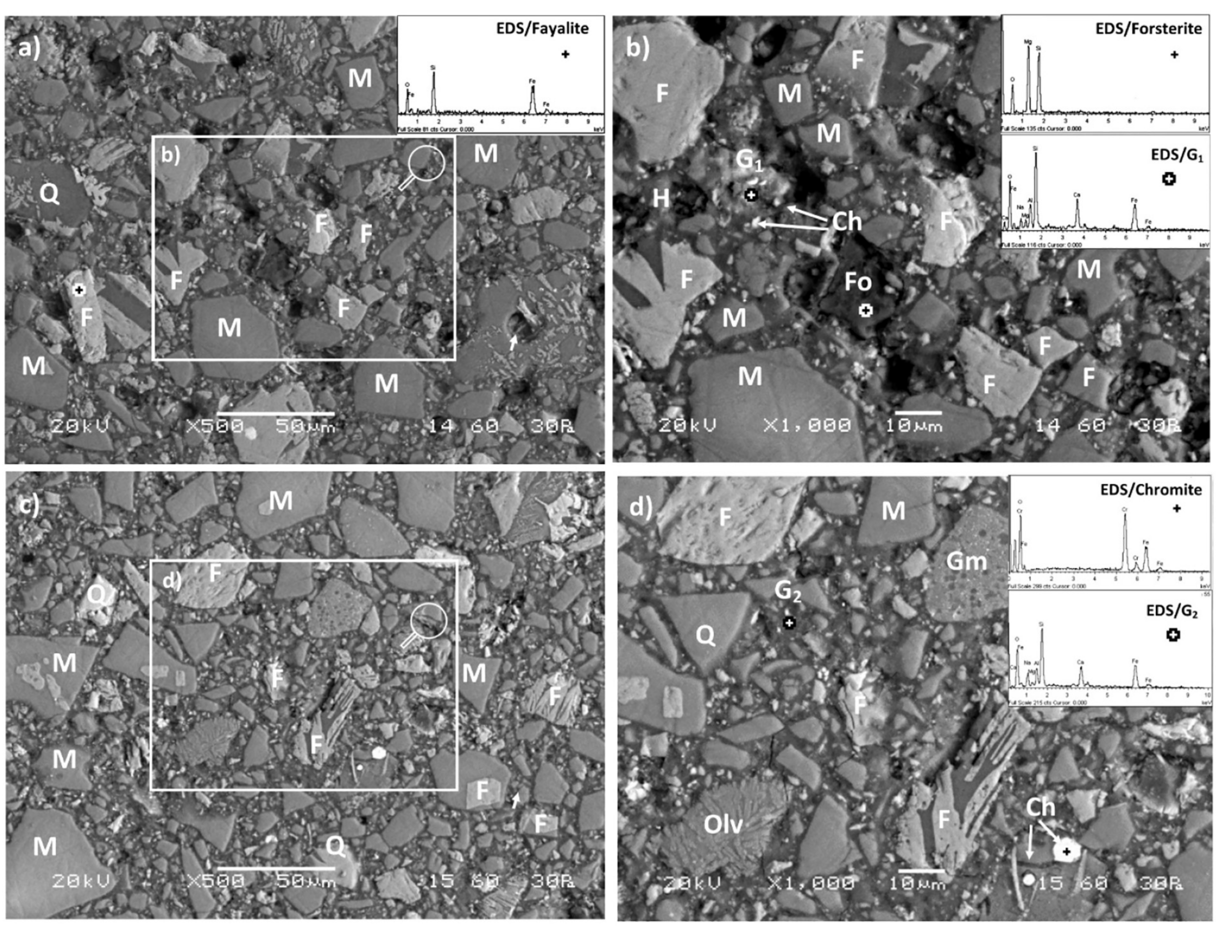


**Fig. 13.** SEM-BSE images of polished cross-sections of selected AAMs (a,b) FS30LS70 and (c,d) FS30LS70 after firing at 250 °C for 6 h. EDS spectra show in several spot locations the presence of metallic and oxide phases, the formation of mixed aggregates and newly formed inorganic gels (Q: Quartz, Fo: Forsterite, F: Fayalite, M: Magnetite, Olv: Olivine, Ch: Chromite, Gm: Glassy matrix, G1:Gel, G2: Gel).

presents a microstructure which is characterized by several holes/pores scattered in the inorganic matrix and a greater proportion of unreacted or partially reacted larger particles compared to FS30LS70 after firing at 250 °C for 6 h.

After firing, it seems that holes were filled with inorganic gel as result of dehydration reactions that took place along with sintering of the unreacted aluminosilicate content (Rincón et al., 2018; Xu et al., 2019) and therefore a denser and more homogenous microstructure was finally formed with a continuous and embedded gel matrix. This well-established microstructure justifies the higher compressive strength obtained for the fired AAM (94 MPa). Fig. 13d (zoom of rectangular area of Fig. 13c) shows in detail the presence of columnar elongated of olivine particles (mixed forsterite/fayalite) and fine to coarse-sized euhedral crystals of anorthite and fayalite embedded in a glassy matrix (Gm) (Lemonis et al., 2015).

## 4. Conclusions

The present study explored the alkali activation potential of fayalitic slags as well as their co-valorization potential, when mixed with ferronickel slag, for the production of AAMs.

The experimental results show that under the synthesis conditions: pre-curing period 24 h, curing temperature 90 °C, curing period 24 h and ageing period 7 days, the maximum values of the compressive strength obtained were 44.8 MPa and 27.2 MPa for FS- and FSP-based AAMs, respectively. The $SiO_2/Na_2O$ molar ratios used in the activating solution were 1.5 and 0.9 in each case, respectively.

The results also show the noticeable co-valorization potential of FS and FSP slags when mixed with LS slag. It is seen that the AAMs produced after alkali activation of FS-LS and FSP-LS mixtures at ratio 50:50, using the same as above synthesis conditions, acquire compressive strength of 64.3 MPa and 45.8 MPa, respectively; the $SiO_2/Na_2O$ molar ratio in the activating solution was 1.0 and 0.9 in each case respectively.

Furthermore, the AAMs produced after alkali activation of slag mixtures maintained sufficient structural integrity after firing for 6 h at temperature up to 500 °C, immersion in distilled water and acidic solution or subjection to freeze-thaw cycles for a period of 7 or 30 days. Finally, all produced AAMs exhibit very low toxicity, as indicated by the application of TCLP, EN 12457-3 and NEN 7341 tests.

The results of this study proved that alkali activation is a viable option for the co-valorization of different slags and the production of AAMs with beneficial properties, thus enabling the minimization of these wastes and the reduction of the environmental footprint of the metallurgical sector.

## CRediT authorship contribution statement

**Konstantinos Komnitsas:** Conceptualization, Methodology, Project administration, Supervision, Writing - review & editing. **Lourdes Yurramendi:** Methodology, Resources, Writing - review & editing. **Georgios Bartzas:** Investigation, Methodology, Data curation, Writing - review & editing. **Vasiliki Karmali:** Investigation, Methodology, Data curation, Writing - original draft. **Evangelos Petrakis:** Investigation, Methodology, Data curation, Writing - original draft.

## Declaration of competing interest

The authors declare that they have no known competing financial interests or personal relationships that could have appeared to influence the work reported in this paper.

## Acknowledgments

The authors would like to acknowledge the financial support of European Commission in the frame of Horizon 2020 project "Metal recovery from low-grade ores and wastes", www.metgrowplus.eu, Grant Agreement n° 690088.

## References

Abdel-Ghani, N.T., Elsayed, A.H., AbdelMoied, S., 2018. Geopolymer synthesis by the alkali-activation of blast furnace steel slag and its fire-resistance. HBRC J. 14 (2), 159–164. https://doi.org/10.1016/j.hbrcj.2016.06.001.

Agnello, A.C., Potysz, A., Fourdrin, C., Huguenot, D., Chauhan, P.S., 2018. Impact of pyrometallurgical slags on sunflower growth, metal accumulation and rhizosphere microbial communities. Chemosphere 208, 626–639. https://doi.org/10.1016/j.chemosphere.2018.06.038.

Alshaaer, M., Zaharaki, D., Komnitsas, K., 2015. Microstructural characteristics and adsorption potential of zeolitic tuff – metakaolin geopolymers. Desalin. Water Treat. 56, 338–345. https://doi.org/10.1080/19443994.2014.938306.

ASTM (American Society for Testing and Materials), 2018. C1262 – 10 Standard Test Method for Evaluating the Freeze-Thaw Durability of Dry Cast Segmental Retaining Wall Units and Related Concrete Units. ASTM International, West Conshohocken, PA 2018. Retrieved from. www.astm.org.

Bartzas, G., Komnitsas, K., 2015. Life cycle assessment of ferronickel production in Greece. Resour. Conserv. Recycl. 105, 113–122. https://doi.org/10.1016/j.resconrec.2015.10.016.

Bernal, S.A., de Gutierrez, R.M., Provis, J.L., Rose, V., 2010. Effect of silicate modulus and metakaolin incorporation on the carbonation of alkali silicate-activated slags. Cem. Concr. Res. 40, 898–907. https://doi.org/10.1016/j.cemconres.2010.02.003.

Bernal, S.A., Provis, J.L., Rose, V., Gutierrez, R.M., 2011. Evolution of binder structure in sodium silicate-activated slag-metakaolin blends. Cem. Concr. Compos. 33, 46–54. https://doi.org/10.1016/j.cemconcomp.2010.09.004.

BSI (British Standards Institute), 2007. BS EN 1936: Natural Stone Test Methods. Determination of Real Density and Apparent Density and of Total and Open Porosity; NP EN 1936:2006. 2007. BSI, London, UK.

Bumanis, G., Novais, R.M., Carvalheiras, J., Bajare, D., Labrincha, J.A., 2019. Metals removal from aqueous solutions by tailored porous waste-based granulated alkali-activated materials. Appl. Clay Sci. 179, 105147. https://doi.org/10.1016/j.clay.2019.105147.

Chen, L., Wang, L., Cho, D.-W., Tsang, D.C.W., Tong, L., Zhou, Y., Yang, J., Hu, Q., Poon, C.S., 2019. Sustainable stabilization/solidification of municipal solid waste incinerator fly ash by incorporation of green materials. J. Clean. Prod. 222, 335–343. https://doi.org/10.1016/j.jclepro.2019.03.057.

Chen, W., Peng, R., Straub, C., Yuan, B., 2020. Promoting the performance of one-part alkali-activated slag using fine lead-zinc mine tailings. Constr. Build. Mater. 236, 117745. https://doi.org/10.1016/j.conbuildmat.2019.117745.

Davidovits, J., 1991. Geopolymers—inorganic polymeric new materials. J. Therm. Anal. Calorim. 37, 1633–1656. https://doi.org/10.1007/BF01912193.

Duxson, P., Provis, J.L., 2008. Designing precursors for geopolymer cements. J. Am. Ceram. Soc. 91, 3864–3869. https://doi.org/10.1111/j.1551-2916.2008.02787.x.

Duxson, P., Provis, J.L., Lukey, G.C., van Deventer, J.S.J., 2007. The role of inorganic polymer technology in the development of 'green concrete'. Cem. Concr. Res. 37, 1590–1597. https://doi.org/10.1016/j.cemconres.2007.08.018.

EN12457-3:2002, 2002. Characterization of Waste – Compliance Test for Leaching of Granular Waste Materials and Sludges – Part 3: Two Stage Batch Test at a Liquid to Solid Ratio of 2 l/kg and 8 l/kg for Materials with High Solid Content and with Particle Size below 4 mm. CEN, Brussels.

Furlani, E., Maschio, S., Magnan, M., Aneggi, E., Andreatta, F., Lekka, M., Lanzutti, A., Fedrizzi, L., 2018. Synthesis and characterization of geopolymers containing blends of unprocessed steel slag and metakaolin: the role of slag particle size. Ceram. Int. 44, 5226–5232. https://doi.org/10.1016/j.ceramint.2017.12.131.

Gao, K., Lin, K.-L., Wang, D., Hwang, C.-L., 2014. Effects $SiO_2/Na_2O$ molar ratio on mechanical properties and the microstructure of nano-$SiO_2$ metakaolin-based geopolymers. Constr. Build. Mater. 53, 503–510. https://doi.org/10.1016/j.conbuildmat.2013.12.003.

Gebregziabiher, B.S., Thomas, R.J., Peethamparan, S., 2016. Temperature and activator effect on early-age reaction kinetics of alkali-activated slag binders. Constr. Build. Mater. 113, 783–793. https://doi.org/10.1016/j.conbuildmat.2016.03.098.

Gee, C., Ramsey, M.H., Maskallh, J., Thornton, I., 1997. Mineralogy and weathering processes in historical smelting slags and their effect on the mobilisation of lead. J. Geochem. Explor. 58, 249–257. https://doi.org/10.1016/s0375-6742(96)00062-3.

Habert, G., Lacaillerie, J.B.E., Russel, N., 2011. An environmental evaluation of geopolymer based concrete production: reviewing current research trends. J. Clean. Prod. 19, 1229–1238. https://doi.org/10.1016/j.jclepro.2011.03.012.

Huang, Y., Wang, Q., Shi, M., 2017. Characteristics and reactivity of ferronickel slag powder. Constr. Build. Mater. 156, 773–789. https://doi.org/10.1016/j.conbuildmat.2017.09.038.

Kaze, C.R., Djobo, J.N.Y., Nana, A., Tchakoute, H.K., Kamseu, E., Melo, U.C., Leonelli, C., Hubert Rahier, H., 2018. Effect of silicate modulus on the setting, mechanical strength and microstructure of iron-rich aluminosilicate (laterite) based-geopolymer cured at room temperature. Ceram. Int. 44 (17), 21442–21450. https://doi.org/10.1016/j.ceramint.2018.08.205.

Khale, D., Chaudhary, R., 2007. Mechanism of geopolymerization and factors influencing its development: a review. J. Mater. Sci. 42, 729–746. https://doi.org/10.1007/s10853-006-0401-4.

Komnitsas, K., 2011. Potential of geopolymer technology towards green buildings and sustainable cities. Procedia Engineering 21, 1023–1032. https://doi.org/10.1016/j.proeng.2011.11.2108.

Komnitsas, K., 2016. Co-valorization of marine sediments and construction & demolition wastes through alkali activation. J. Environ. Chem. Eng. 4, 4661–4669. https://doi.org/10.1016/j.jece.2016.11.003.

Komnitsas, K., Zaharaki, D., 2007. Geopolymerisation. A review and prospects for the minerals industry. Miner. Eng. 20, 1261–1277. https://doi.org/10.1016/j.mineng.2007.07.011.

Komnitsas, K., Zaharaki, D., Perdikatsis, V., 2007. Geopolymerisation of low calcium ferronickel slags. J. Mater. Sci. 42 (9), 3073–3082. https://doi.org/10.1007/s10853-006-0529-2.
Komnitsas, K., Zaharaki, D., Perdikatsis, V., 2009. Effect of synthesis parameters on the compressive strength of low-calcium ferronickel slag inorganic polymers. J. Hazard. Mater. 161, 760–768. https://doi.org/10.1016/j.jhazmat.2008.04.055.
Komnitsas, K., Zaharaki, D., Bartzas, G., 2013. Effect of sulphate and nitrate anions on heavy metal immobilisation in ferronickel slag geopolymers. Appl. Clay Sci. 73, 103–109. https://doi.org/10.1016/j.clay.2012.09.018.
Komnitsas, K., Zaharaki, D., Vlachou, A., Bartzas, G., Galetakis, M., 2015. Effect of synthesis parameters on the quality of construction and demolition wastes (CDW) geopolymers. Adv. Powder Technol. 26, 368–376. https://doi.org/10.1016/j.apt.2014.11.012.
Komnitsas, K., Bartzas, G., Karmali, V., Petrakis, E., Kurylak, W., Pietek, G., Kanasiewicz, J., 2019a. Assessment of alkali activation potential of a Polish ferronickel slag. Sustainability 11, 1863. https://doi.org/10.3390/su11071863.
Komnitsas, K., Petrakis, E., Bartzas, G., Karmali, V., 2019b. Column leaching of low-grade saprolitic laterites and valorization of leaching residues. Sci. Tot. Environ. 665, 347–357. https://doi.org/10.1016/j.scitotenv.2019.01.381.
Kriven, W.M., Bell, J.L., Gordon, M., 2003. Microstructure and microchemistry of fully-reacted geopolymers and geopolymer matrix composites. Ceram. Trans. 153, 227–250. https://doi.org/10.1002/9781118406892.ch15.
Krivenko, P.V., Kovalchuk, G.Y., 2007. Directed synthesis of alkaline aluminosilicate minerals in a geocement matrix. J. Mater. Sci. 42, 2944–2952. https://doi.org/10.1007/s10853-006-0528-3.
Lee, W.K.W., van Deventer, J.S.J., 2002. The effects of inorganic salt contamination on the strength and durability of geopolymers. Colloids Surf. A. Physicochem. Eng. Aspects 211, 115–126. https://doi.org/10.1016/s0927-7757(02)00239-x.
Lemonis, N., Tsakiridis, P.E., Katsiotis, N.S., Antiohos, S., Papageorgiou, D., Katsiotis, M.S., Beazi-Katsioti, M.S., 2015. Hydration study of ternary blended cements containing ferronickel slag and natural pozzolan. Constr. Build. Mater. 81, 130–139. https://doi.org/10.1016/j.conbuildmat.2015.02.046.
Li, Q., Yang, Y., Yang, K., Chao, Z., Tang, D., Tian, Yi, Wu, F., Basheer, M., Yang, C., 2019. The role of calcium stearate on regulating activation to form stable, uniform and flawless reaction products in alkali-activated slag cement. Cem. Concr. Res. 103, 242–251. https://doi.org/10.1016/j.cemconcomp.2019.05.009.
Liu, Z., Wang, J., Jiang, Q., Cheng, G., Li, L., Kang, Y., Wang, D., 2019. A green route to sustainable alkali-activated materials by heat and chemical activation of lithium slag. J. Clean. Prod. 225, 1184–1193. https://doi.org/10.1016/j.jclepro.2019.04.018.
Luukkonen, T., Abdollahnejad, Z., Yliniemi, J., Kinnunyn, P., Illikainen, M., 2018. Comparison of alkali and silica sources in one-part alkali-activated blast furnace slag mortar. J. Clean. Prod. 187, 171–179. https://doi.org/10.1016/j.jclepro.2018.03.202.
Luukkonen, T., Heponiemi, A., Runtti, H., Pesonen, A., Yliniemi, J., Lassi, U., 2019. Application of alkali-activated materials for water and wastewater treatment: a review. Rev. Environ. Sci. Biotechnol. 18 (2), 271–297. https://doi.org/10.1007/s11157-019-09494-0.
Maragkos, I., Giannopoulou, P.I., Panias, D., 2009. Synthesis of ferronickel slag-based geopolymers. Miner. Eng. 22, 196–203. https://doi.org/10.1016/j.mineng.2008.07.003.
Marjanović, J.N., Komljenović, M., Baščarević, Z., Nikolić, V., Petrović, R., 2015. Physical-mechanical and microstructural properties of alkali-activated fly ash-blast furnace slag blends. Ceram. Int. 41, 1421–1435. https://doi.org/10.1016/j.ceramint.2014.09.075.
Mastali, M., Shaad, K.M., Abdollahnejad, Z., Falah, M., Kinnunen, P., Illikainen, M., 2020. Towards sustainable bricks made with fiber-reinforced alkali-activated desulfurization slag mortars incorporating carbonated basic oxygen furnace aggregates. Constr. Build. Mater. 232, 117258. https://doi.org/10.1016/j.conbuildmat.2019.117258.
Mohamed, O.A., 2019. A review of durability and strength characteristics of alkali-activated slag concrete. Materials 12 (8), 1198. https://doi.org/10.3390/ma12081198.
Muñoz, I., Cifrian, E., Andrés, A., SanMiguel, G., Ruiz, D., Viguri, J.R., 2018. Analysis of environmental benefits associated with the incorporation of Waelz slag into fired bricks using LCA. Constr. Build. Mater. 168, 178–186. https://doi.org/10.1016/j.conbuildmat.2018.02.108.
Muthuvel, I., Gowthami, K., Thirunarayanan, G., Suppuraj, P., Krishnakumar, B., do Nascimento Sobral, J.F., Swaminathan, M., 2019. Graphene oxide–Fe2V4O13 hybrid material as highly efficient hetero-Fenton catalyst for degradation of methyl orange. Int. J. Ind. Chem. 10, 1–11. https://doi.org/10.1007/s40090-019-0173-8.
NEN 7341, 1995. Leaching Characteristics of Solid Earthy and Stony Building and Waste Materials-leaching Tests: Determination of the Availability of Inorganic Components for Leaching. 1st ed. Nederlands Normalisatie Instituut (NNI), Delft, the Netherlands ICS 13.030-70;91.100.
Onisei, S., Pontikes, Y., Van Gerven, T., Angelopoulos, G.N., Velea, T., Predica, V., Moldovan, P., 2012. Synthesis of inorganic polymers using fly ash and primary lead slag. J. Hazard. Mater. 205–206, 101–110. https://doi.org/10.1016/j.jhazmat.2011.12.039.
Ouellet-Plamondon, C., Habert, G., 2014. Life cycle analysis (LCA) of alkali-activated cements and concretes. Handbook of Alkali-activated Cements, Mortars and Concretes. WoodHead Publishing-Elsevier, Cambridge, pp. 663–686.
Pacheco-Torgal, F., Abdollahnejad, Z., Miraldo, S., Kheradmand, M., 2017. Alkali-activated cement-based binders (AACBs) as durable and cost-competitive low-$CO_2$ binder materials: some shortcomings that need to be addressed, chapter 9. Handbook of Low Carbon Concrete. Butterworth-Heinemann, Oxford, pp. 195–216. https://doi.org/10.1016/B978-0-12-804524-4.00009-9.
Palomo, A., Krivenko, P., Garcia-Lodeiro, I., Kavalerova, E., Maltseva, O., Fernández-Jiménez, A., 2014. A review on alkaline activation: new analytical perspectives. Mater. Constr. 64 (315), 22. https://doi.org/10.3989/mc.2014.00314.
Pasetto, M., Baliello, A., Giacomello, G., Pasquini, E., 2017. Sustainable solutions for road pavements: a multi-scale characterization of warm mix asphalts containing steel slags. J. Clean. Prod. 166, 835–843. https://doi.org/10.1016/j.jclepro.2017.07.212.
Passuello, A., Rodríguez, E.D., Hirt, E., Longhi, M., Bernal, S.A., Provis, J.L., 2017. Evaluation of the potential improvement in the environmental footprint of geopolymers using waste-derived activators. J. Clean. Prod. 166, 680–689. https://doi.org/10.1016/j.jclepro.2017.08.007.
Petrakis, E., Karmali, V., Bartzas, G., Komnitsas, K., 2019. Grinding kinetics of slag and effect of final particle size on the compressive strength of alkali activated materials. Minerals 9, 714. https://doi.org/10.3390/min9110714.
Peys, A., Douvalis, A.P., Siakati, C., Rahier, H., Blanpain, B., Pontikes, Y., 2019a. The influence of air and temperature on the reaction mechanism and molecular structure of Fe-silicate inorganic polymers. J. Non-Cryst. Solids 526, 119675. https://doi.org/10.1016/j.jnoncrysol.2019.119675.
Peys, A., Douvalis, A.P., Hallet, V., Rahier, H., Blanpain, B., Pontikes, Y., 2019b. Inorganic polymers from CaO-FeOx-$SiO_2$ Slag: the start of oxidation of Fe and the formation of a mixed valence binder. Front. Mater. Sci. 6, 212. https://doi.org/10.3389/fmats.2019.00212.
Pontikes, Y., Machiels, L., Onisei, S., Pandelaers, L., Geysen, D., Jones, P.T., Blanpain, B., 2013. Slags with a high Al and Fe content as precursors for inorganic polymers. Appl. Clay Sci. 73, 93–102. https://doi.org/10.1016/j.clay.2012.09.020.
Provis, J.L., Bernal, S.A., 2014. Geopolymers and related alkali-activated materials. Annu. Rev. Mater. Res. 44, 229–327. https://doi.org/10.1146/annurev-matsci-070813-113515.
Ravikumar, D., Neithalath, N., 2012. Effects of activator characteristics on the reaction product formation in slag binders activated using alkali silicate powder and NaOH. Cem. Concr. Compos. 34, 809–818. https://doi.org/10.1016/j.cemconcomp.2012.03.006.
Rincón, A., Desideri, D., Bernardo, E., 2018. Functional glass-ceramic foams from 'inorganic gel casting' and sintering of glass/slag mixtures. J. Clean. Prod. 187, 250–256. https://doi.org/10.1016/j.jclepro.2018.03.065.
Saari, V., Latostenmaa, P., Yliniemi, J., Ohenoja, K., 2019. Boliden Harjavalta copper and nickel smelter – review of smelter operations, slags and slag valorization studies. $6^{th}$ International Slag Valorisation Symposium, 1–5 April 2019, Mechelen, Belgium Retrieved from. www.slag-valorisation-symposium.eu.
Shi, C., Qu, B., Provis, J.L., 2019. Recent progress in low-carbon binders. Cem. Concr. Res. 122, 227–250. https://doi.org/10.1016/j.cemconres.2019.05.009.
Sindhunata van Deventer, J.S.J., Lukey, G.C., Xu, H., 2006. Effect of curing temperature and silicate concentration on fly-ash-based geopolymerization. Ind. Eng. Chem. Res. 45, 3559–3568. https://doi.org/10.1021/ie051251p.
Soultana, A., Valouma, A., Bartzas, G., Komnitsas, K., 2019. Properties of inorganic polymers produced form brick waste and metallurgical slag. Minerals 9, 551. https://doi.org/10.3390/min9090551.
Tchadjie, L.N., Ekolu, S.O., 2018. Enhancing the reactivity of aluminosilicate materials toward geopolymer synthesis. Mater. Sci. 53, 4709–4733. https://doi.org/10.1007/s10853-017-1907-7.
Traven, K., Češnovar, M., Ducman, V., 2019. Particle size manipulation as an influential parameter in the development of mechanical properties in electric arc furnace slag-based AAM. Ceram. Int. 45 (17), 22632–22641. https://doi.org/10.1016/j.ceramint.2019.07.296.
US EPA, 1992. TCLP (Toxicity Characteristics Leaching Procedure), Method 1311, Revision 2, July 1992.
Van De Sande, J., Peys, A., Hertel, T., Rahier, H., Pontikes, Y., 2020. Upcycling of non-ferrous metallurgy slags: identifying the most reactive slag for inorganic polymer construction materials. Resour. Conserv. Recycl. 154, 104627. https://doi.org/10.1016/j.resconrec.2019.104627.
Wang, L., Chen, L., Tsang, D.C.W., Zhou, Y., Rinklebe, J., Song, H., Kwon, E.E., Baek, K., Ok, Y.S., 2019. Mechanistic insights into red mud, blast furnace slag, or metakaolin-assisted stabilization/solidification of arsenic-contaminated sediment. Environ. Int. 133, 105247. https://doi.org/10.1016/j.envint.2019.105247.
Xu, H., Van Deventer, J.S.J., 2000. The geopolymerisation of alumino-silicate minerals. Int. J. Miner. Process. 59, 247–266. https://doi.org/10.1016/s0301-7516(99)00074-5.
Xu, Y., Yang, B., Liu, X., Gao, S., Li, D., Mukiza, E., Li, H., 2019. Investigation of the medium calcium based non-burnt brick made by red mud and fly ash: durability and hydration characteristics. Int. J. Min. Met. Mater. 26, 983. https://doi.org/10.1007/s12613-019-1814-9.
Yan, B., Yu, Q.L., Brouwers, H.J.H., 2017. Evaluation of slag characteristics on the reaction kinetics and mechanical properties of $Na_2CO_3$ activated slag. Constr. Build. Mater. 131, 334–346. https://doi.org/10.1016/j.conbuildmat.2016.11.074.
Yip, C.K., Lukey, G.C., van Deventer, J.S.J., 2005. The coexistence of geopolymeric gel and calcium silicate hydrate at the early stage of alkaline activation. Cem. Concr. Res. 35, 1688–1697. https://doi.org/10.1016/j.cemconres.2004.10.042.
Yip, C.K., Lukey, G.C., Provis, J.L., Van Deventer, J.S.J., 2008. Effect of calcium silicate sources on geopolymerisation. Cem. Concr. Res. 38, 554–564. https://doi.org/10.1016/j.cemconres.2007.11.001.
Yuan, J., He, P., Jia, D., Yang, C., Zhang, Y., Yan, S., Yang, Z., Duan, X., Wang, S., Zhou, Y., 2016. Effect of curing temperature and $SiO_2/K_2O$ molar ratio on the performance of metakaolin-based geopolymers. Ceram. Int. 42, 16184–16190. https://doi.org/10.1016/j.ceramint.2016.07.139.
Zaharaki, D., Komnitsas, K., 2009. Effect of additives on the compressive strength of slag-based inorganic polymers. Glob. Nest J. 11, 137–146. https://doi.org/10.30955/gnj.000585.
Zaharaki, D., Komnitsas, K., 2012. Long term behaviour of ferronickel slag inorganic polymers in various environments. Fresenius Environ. Bull. 21, 2436–2440.
Zaharaki, D., Komnitsas, K., Perdikatsis, V., 2010. Use of analytical techniques for identification of inorganic polymer gel composition. J. Mater. Sci. 45, 2715–2724. https://doi.org/10.1007/s10853-010-4257-2.
Zaharaki, D., Galetakis, M., Komnitsas, K., 2016. Valorization of construction and demolition (C&D) and industrial wastes through alkali activation. Constr. Build. Mater. 121, 686–693. https://doi.org/10.1016/j.conbuildmat.2016.06.051.
Zhang, Z.H., Yao, X., Zhu, H.J., 2009. Role of water in the synthesis of calcined kaolin-based geopolymer. Appl. Clay Sci. 43, 218–223. https://doi.org/10.1016/j.clay.2008.09.003.